**Proceedings of the 7th International Symposium on Cavitation**
**CAV2009- Paper No.18**
**August 17-22, 2009, Ann Arbor, Michigan, USA**

# UNSTEADY BUBBLY CAVITATING NOZZLE FLOWS

**Can F. Delale**
Istanbul Technical University
Istanbul, Turkey

**Zafer Başkaya**
Istanbul Technical University
Istanbul, Turkey

**Steffen J. Schmidt**
Technische Universität München
Garching, Germany

**Günter H. Schnerr**
Technische Universität München
Garching, Germany

## ABSTRACT

Unsteady quasi-one-dimensional and two-dimensional cavitating nozzle flows are considered using a homogeneous bubbly flow model. For quasi-one-dimensional nozzle flows, the system of model equations is reduced to two evolution equations for the flow speed and bubble radius and the initial and boundary value problems for the evolution equations are formulated. Results obtained for quasi-one-dimensional nozzle flows capture the measured pressure losses due to cavitation, but they turn out to be insufficient in describing the two-dimensional structures. For this reason, model equations for unsteady two-dimensional bubbly cavitating nozzle flows are considered and, by suitable decoupling, they are reduced to evolution equations for the bubble radius and for the velocity field, the latter being determined by an integro-partial differential system for the unsteady acceleration. This integro-partial differential system constitutes the fundamental equations for the evolution of the dilation and vorticity in two-dimensional cavitating nozzle flows. The initial and boundary value problem of the evolution equations are then discussed and a method to integrate the equations is introduced. Due to a lack of an algorithm to compute two-dimensional bubbly cavitating flows presently, the numerical simulation of 2D cavitating nozzle flows is obtained by the CFD-Tool CATUM, which is based on an equilibrium phase transition model. Results obtained for a typical cavitation cycle show instantaneous high pressure pulses at instances of cloud collapses.

## INTRODUCTION

Cavitating flows through converging-diverging nozzles have direct applications in ducts and venturi tubes as well as in Diesel injection nozzles. The first model of bubbly liquid flow through a converging-diverging nozzle was proposed by Tangren et al. [1] using a barotropic model. The problem has been reconsidered by Ishii et al. [2] by taking into account unsteady effects, but still neglecting bubble dynamics. A one-dimensional continuum bubbly flow model that couples spherical bubble dynamics to the flow equations was proposed by van Wijngaarden [3,4] and was later employed in investigating shock wave structure [5]. Quasi-one-dimensional steady-state solutions of bubbly cavitating flows through converging-diverging nozzles have also been investigated using the continuum bubbly mixture model [6,7] by assuming that the gas pressure inside the bubble obeys the polytropic law and by lumping all damping mechanisms by a single damping coefficient in the form of viscous dissipation. These investigations have demonstrated that steady-state solutions are possible only for some range of the cavitation number, with the rest of the parameters kept fixed. Moreover, a recent investigation [8] shows that the temporal stability of these quasi-one-dimensional steady-state solutions suffer from being very sensitive to slight unsteady perturbations. A numerical investigation of unsteady quasi-one-dimensional bubbly cavitating flows have also been carried out [9] showing the possibility of propagating bubbly shock waves in the diverging section of the nozzle.

The aim of this investigation is to give a detailed qualitative as well as quantitative analysis of unsteady quasi-one-dimensional and two-dimensional cavitating nozzle flows. For this reason we first discuss the homogeneous bubbly flow model previously introduced for quasi-one-dimensional steady-state and unsteady cavitating nozzle flows [5-9]. In this case, the system of model equations is reduced to two evolution equations for the flow speed and bubble radius and the initial and boundary value problems for the evolution equations are formulated. In this case a numerical algorithm is constructed for the solution of the initial and boundary value problems of evolution equations. Results obtained for quasi-one-dimensional nozzle flows capture the measured pressure losses due to cavitation, but they turn out to be insufficient in describing the two-dimensional structures such as the formation

and development of the attached cavity, the formation of the re-entrant jet and bubble cloud shedding and collapse. For this reason model equations for unsteady two-dimensional bubbly cavitating nozzle flows are considered and, by suitable decoupling, are reduced to evolution equations for the bubble radius and for the velocity field, the latter being determined by an integro-partial differential system for the unsteady acceleration. More importantly, this integro-algebraic partial differential system seems to form the fundamental equations for the evolution of the dilation and vorticity. In particular, the evolution equation of vorticity is shown to be precisely Fridman's equation of vorticity [10], containing terms arising from non-barotropic flow. The initial and boundary value problem of the evolution equations are then discussed and a method to integrate the equations is introduced. Unfortunately, the quantitative results of such a numerical algorithm are not yet available. Therefore, the quantitative results for 2D flows were obtained by an equilibrium phase transition cavitation model algorithm (CATUM), which has especially proved fruitful in capturing wave dynamics [11-14]. Results obtained for a typical cavitation cycle show instantaneous high pressure pulses at instances of cloud collapses.

## MODEL EQUATIONS FOR UNSTEADY BUBBLY CAVITATING NOZZLE FLOWS

In this section we introduce the quasi-one-dimensional and the two-dimensional model equations of bubbly cavitating nozzle flows.

### A. QUASI-ONE-DIMENSIONAL FLOWS

We consider an unsteady quasi-one-dimensional cavitating nozzle flow and we assume that the initial distributions, inlet conditions and nozzle geometry are such that cavitation can occur in the nozzle. We use a slightly modified version of the homogeneous bubbly mixture model [3-9]. In this model the slip between the bubbles and the liquid as well as the creation (nucleation and bubble fission) and coagulation of bubbles are neglected and spherical bubbles are assumed. These assumptions have been specifically addressed [15-22] and can be taken into account by an improved model. The quasi-one-dimensional unsteady nozzle flow equations then take the form

$$\rho' = \rho_\ell'(1-\beta) \tag{1}$$

$$A'\frac{\partial \rho'}{\partial t'} + \frac{\partial}{\partial x'}(\rho' u' A') = 0 \tag{2}$$

$$\rho'\frac{du'}{dt'} = -\frac{\partial p'}{\partial x'} \tag{3}$$

$$\frac{R'^3(1-\beta)}{\beta} = \frac{3}{4\pi\eta_0'} = \text{constant} \tag{4}$$

The above equations are supplemented by a modified Rayleigh-Plesset equation for spherical bubble dynamics, which takes bubble/bubble interactions into account in the mean-field as

$$\frac{p_v' - p'}{\rho_\ell'} = \frac{\left[1+(2/3)\pi\eta_0'(3\Lambda^2-1)R'^3\right]}{\left[1+(4/3)\pi\eta_0' R'^3\right]^2} R'\frac{d^2R'}{dt'^2}$$

$$+\frac{3}{2}\frac{\left[1+(8/3)\pi\eta_0'(2\Lambda^2-1)R'^3+(16/9)\pi^2\eta_0'^2\Lambda^2R'^6\right]}{\left[1+(4/3)\pi\eta_0' R'^3\right]^2}\left(\frac{dR'}{dt'}\right)^2$$

$$+\frac{2S'}{\rho_\ell' R'} + \frac{4\mu_{eff}'}{\rho_\ell' R'}\frac{dR'}{dt'} - p_{gi}'\left(\frac{R_0'}{R'}\right)^{3k} \tag{5}$$

where $\Lambda$ denotes the bubble/bubble interaction parameter defined by

$$\Lambda = \frac{\Delta r'}{R'} \tag{6}$$

with $\Delta r'$ denoting the radius of influence of interacting bubbles from the center of any fixed bubble [7,23]. In eq. (5) a polytropic law for the expansion and compression of the gas inside the gas/vapor bubble is used and all damping mechanisms, in an *ad hoc* manner, [24-27] are assumed in the form of viscous dissipation, characterized by a single viscosity coefficient $\mu_{eff}'$. Using the normalization

$$\rho = \frac{\rho}{\rho_\ell'} = 1-\beta,\ \ p = \frac{p'}{p_{i0}'},\ \ p_v = \frac{p_v'}{p_{i0}'},$$

$$p_g = \frac{p_g'}{p_{i0}'},\ \ u = \frac{u'}{\sqrt{p_{i0}'/\rho_\ell'}}$$

$$x = \frac{x'}{H_i'},\ \ A = \frac{A'}{A_i'},\ \ t = \frac{t'}{\Theta'} = \frac{\sqrt{p_{i0}'/\rho_\ell'}\,t'}{H_i'},\ \ R = \frac{R'}{R_{i0}'}, \tag{7}$$

eqs. (1)-(5) take the normalized form

$$\rho = 1-\beta, \tag{8}$$

$$A\frac{\partial \rho}{\partial t} + \frac{\partial}{\partial x}(\rho u A) = 0, \tag{9}$$

$$\rho\frac{du}{dt} = -\frac{\partial p}{\partial x}, \tag{10}$$

$$R^3\left(\frac{1-\beta}{\beta}\right)=\frac{1-\beta_{i0}}{\beta_{i0}}=\kappa_i^3 \qquad (11)$$

and

$$\frac{p_v-p}{L^2}=\frac{\left[1+(3\Lambda^2-1)(R/\kappa_i)^3/2\right]}{\left[1+(R/\kappa_i)^3\right]}R\frac{d^2R}{dt^2}$$

$$+\frac{3}{2}\frac{\left[1+2(2\Lambda^2-1)(R/\kappa_i)^3+\Lambda^2(R/\kappa_i)^6\right]}{\left[1+(R/\kappa_i)^3\right]^2}\left(\frac{dR}{dt}\right)^2$$

$$+\frac{S_0}{L^2R}+\frac{4}{L^2(\mathrm{Re})R}\frac{dR}{dt}-\frac{p_{gi}}{L^2R^{3k}} \qquad (12)$$

where $L$ is the ratio of micro scale to macro scale defined by

$$L=\frac{R'_{i0}}{H'_i}\ , \qquad (13)$$

$\kappa_i$ is a parameter defined in terms of the inlet void fraction $\beta_i$ by

$$\kappa_i^3=\frac{1-\beta_{i0}}{\beta_{i0}}\ , \qquad (14)$$

$S_0$ is the non-dimensional surface tension coefficient defined by

$$S_0=\frac{2S'}{p'_{i0}R'_{i0}}\ , \qquad (15)$$

and Re is a typical Reynolds number, based on the overall damping coefficient $\mu'_{eff}$, and is defined by

$$\mathrm{Re}=\frac{\rho'_\ell H'_i\sqrt{p'_{i0}/\rho'_\ell}}{\mu'_{eff}}\ . \qquad (16)$$

Furthermore, by eliminating the void fraction $\beta$, the mixture density ρ and the mixture pressure $p$ between eqs. (8)-(12), we arrive at the evolution equations for the bubble radius $R(x,t)$ and for the flow speed $u(x,t)$ as

$$\frac{\partial R}{\partial t}=-u\frac{\partial R}{\partial x}+\frac{1}{3R^2}(R^3+\kappa_i^3)\left[\left(\frac{1}{A}\frac{dA}{dx}\right)u+\frac{\partial u}{\partial x}\right] \qquad (17)$$

and

$$\frac{\partial u}{\partial t}=a(x,t) \qquad (18)$$

where the unsteady acceleration satisfies the linear partial differential equation

$$\frac{\partial^2 a}{\partial x^2}+g(R,\frac{\partial R}{\partial x},x)\frac{\partial a}{\partial x}+h(R,\frac{\partial R}{\partial x},x)a$$

$$=s(R,u,\frac{\partial R}{\partial x},\frac{\partial u}{\partial x},\frac{\partial^2 u}{\partial x^2},\frac{\partial^3 u}{\partial x^3},x) \qquad (19)$$

where the functions g, h, and s are given by

$$g(R,\frac{\partial R}{\partial x},x)=\frac{F_1(R)}{F_2(R)}\frac{\partial R}{\partial x}+\frac{1}{A}\frac{dA}{dx}\ , \qquad (20)$$

$$h(R,\frac{\partial R}{\partial x},x)=\frac{F_1(R)}{F_2(R)}\left(\frac{1}{A}\frac{dA}{dx}\right)\frac{\partial R}{\partial x}+\frac{F_3(R)}{F_2(R)}+\frac{d}{dx}\left(\frac{1}{A}\frac{dA}{dx}\right) \qquad (21)$$

and

$$s(R,u,\frac{\partial R}{\partial x},\frac{\partial u}{\partial x},\frac{\partial^2 u}{\partial x^2},\frac{\partial^3 u}{\partial x^3},x)=-\Bigg\{u\frac{\partial^3 u}{\partial x^3}$$

$$+\left[\frac{F_1(R)}{F_2(R)}u\frac{\partial R}{\partial x}+\frac{F_4(R)}{F_2(R)}\frac{\partial u}{\partial x}+\frac{F_4(R)}{F_2(R)}u\left(\frac{1}{A}\frac{dA}{dx}\right)+\frac{F_5(R)}{F_2(R)}\right]\frac{\partial^2 u}{\partial x^2}$$

$$+\frac{F_6(R)}{F_2(R)}\frac{\partial R}{\partial x}\left(\frac{\partial u}{\partial x}\right)^2$$

$$+\left[\frac{F_7(R)}{F_2(R)}\left(\frac{1}{A}\frac{dA}{dx}\right)-3\frac{F_3(R)F_5(R)}{RF_2(R)}\right]\frac{\partial R}{\partial x}\frac{\partial u}{\partial x}$$

$$+\frac{F_4(R)}{F_2(R)}\left(\frac{1}{A}\frac{dA}{dx}\right)\left(\frac{\partial u}{\partial x}\right)^2+\left[\frac{F_8(R)}{F_2(R)}u\frac{d}{dx}\left(\frac{1}{A}\frac{dA}{dx}\right)\right.$$

$$\left.+\frac{F_9(R)}{F_2(R)}u\left(\frac{1}{A}\frac{dA}{dx}\right)^2+\frac{F_5(R)}{F_2(R)}\left(\frac{1}{A}\frac{dA}{dx}\right)+\frac{F_3(R)}{F_2(R)}u\right]\frac{\partial u}{\partial x}$$

$$+\left[\frac{F_6(R)}{F_2(R)}u^2\left(\frac{1}{A}\frac{dA}{dx}\right)^2-3\frac{F_3(R)F_5(R)}{RF_2(R)}u\left(\frac{1}{A}\frac{dA}{dx}\right)\right.$$

$$\left.+\frac{F_1(R)}{F_2(R)}u^2\frac{d}{dx}\left(\frac{1}{A}\frac{dA}{dx}\right)+\frac{F_{10}(R)}{F_2(R)}\right]\frac{\partial R}{\partial x}$$

$$+\frac{F_9(R)}{F_2(R)}u^2\left(\frac{1}{A}\frac{dA}{dx}\right)\frac{d}{dx}\left(\frac{1}{A}\frac{dA}{dx}\right)+u^2\frac{d^2}{dx^2}\left(\frac{1}{A}\frac{dA}{dx}\right)$$

$$+\frac{F_5(R)}{F_2(R)}u\frac{d}{dx}\left(\frac{1}{A}\frac{dA}{dx}\right)+\frac{\partial p_v/\partial x}{F_2(R)}\Bigg\} \qquad (22)$$

The functions $F_j\ (R)$ ; j=1,2,...,10 , entering eqs. (20)-(22) are given in appendix A. The solution for the mixture pressure, the void fraction and the density then follow by

$$p = p_v - \frac{S_0}{R} + \frac{p_{gi}}{R^{3k}} - \frac{L^2\kappa_i^6}{18R^4}\Big[(6\Lambda^2-1)(R/\kappa_i)^6$$

$$+(6\Lambda^2-2)(R/\kappa_i)^3-1\ \Big]\ \psi^2$$

$$-\frac{4\kappa_i^3}{3(\mathrm{Re})R^3}\Big[1+(R/\kappa_i)^3\Big]\psi$$

$$-\frac{L^2\kappa_i^3}{6R}\Big[2+(3\Lambda^2-1)(R/\kappa_i)^3\Big]\frac{d\psi}{dt} \qquad (23)$$

and

$$\beta = 1-\rho = \frac{R^3}{R^3+\kappa_i^3} \qquad (24)$$

where the dilation $\Psi$ is defined by $\Psi=\partial u/\partial x+(1/A\ dA/dx)u$ . In particular, eq. (23) is independent of flow dimensionality and may be helpful for a quantitative comparison of the pressure distributions obtained by different cavitation models, whether they are based on barotropic relations or phase transition models. The steady-state solutions of the model equations are obtained if, in addition to the vanishing of the unsteady acceleration ($a$=0), ∂R/∂t also vanishes everywhere for all times. In such a case we precisely recover the steady-state solution [7]. The single-phase incompressible steady-state limit is also achieved when $\kappa_i$ >>1 and R is of O(1) on measure $\kappa_i$. If we define a small parameter ε by

$$\varepsilon = \frac{1}{\kappa_i^3}\ , \qquad (25)$$

the steady-state continuity and momentum equations in the incompressible limit become

$$\bar{u} = \frac{u_i}{A}\Big[1+\varepsilon(\bar{R}^3-1)+O(\varepsilon^2)\Big] \qquad (26)$$

$$\frac{d}{dx}\left[\bar{p}+\frac{1}{2}\bar{u}^2\right] = \varepsilon\bar{R}^3\frac{d\bar{u}}{dx}+O(\varepsilon^2) \qquad (27)$$

where $u_i$ is the initial normalized inlet flow speed and $\bar{(\ )}$ denotes steady-state variables. Equations (26) and (27) show that deviations from the single-phase incompressible solution can hardly be observed as long as R remains of O(1) on measure ε. Equations (26) and (27) show that the steady-state incompressible flow solution is violated only when R becomes of O(ε $^{-1/3}$) (the cavitating flow regime). In particular, in the limit as $\kappa_i \to\infty$ (i.e. ε →0 which implies that R→0 and, consequently, $\beta$→0, eq. (26) reduces to the incompressible single-phase velocity distribution and eq. (27) yields Bernoulli's equation.

### B. TWO-DIMENSIONAL FLOWS

For the analysis of the 2D (or 3D) structures of partial cavitation and supercavitation observed in experiments, the quasi-one-dimensional model equations discussed above are insufficient. Therefore, the model equations should be extended to multi-dimensional flows. In this section, for simplicity, we introduce the model equations for two-dimensional unsteady bubbly cavitating flows to be able to calculate, at least, some of the 2-D flow structures observed. Using the homogeneous two-phase dispersed flow model and the classical Euler equations, the continuity and momentum equations in two-dimensions take the form

$$\frac{\partial\rho'}{\partial t'}+\frac{\partial}{\partial x'}\left(\rho'u'\right)+\frac{\partial}{\partial y'}\left(\rho'v'\right)=0\ , \qquad (28)$$

$$\rho'\left(\frac{\partial u'}{\partial t'}+u'\frac{\partial u'}{\partial x'}+v'\frac{\partial u'}{\partial y'}\right)=-\frac{\partial p'}{\partial x'} \qquad (29)$$

and

$$\rho'\left(\frac{\partial v'}{\partial t'}+u'\frac{\partial v'}{\partial x'}+v'\frac{\partial v'}{\partial y'}\right)=-\frac{\partial p'}{\partial y'} \qquad (30)$$

where the mixture density $\rho'$ is given by eq. (1) and the void fraction $\beta$ is related to the radius of mono-dispersed spherical bubbles by eq. (4), assuming there is no bubble creation and coagulation. Equations (28)-(30) together with eqs. (1), (4) and the modified Rayleigh-Plesset equation (5) constitute the model equations for unsteady 2-D bubbly cavitating nozzle flows. With the normalization given by eq. (7) together with $y=y'/H'_i$ , the two-dimensional normalized model equations take the form

$$\rho=\left(1-\beta\right), \qquad (31)$$

$$\frac{\partial\rho}{\partial t}+\frac{\partial}{\partial x}\left(\rho u\right)+\frac{\partial}{\partial y}\left(\rho v\right)=0\ , \qquad (32)$$

$$\rho\left(\frac{\partial u}{\partial t}+u\frac{\partial u}{\partial x}+v\frac{\partial u}{\partial y}\right)=-\frac{\partial p}{\partial x}, \qquad (33)$$

$$\rho\left(\frac{\partial v}{\partial t}+u\frac{\partial v}{\partial x}+v\frac{\partial v}{\partial y}\right)=-\frac{\partial p}{\partial y}, \qquad (34)$$

and

$$R^3 \frac{1-\beta}{\beta} = \frac{1-\beta_i}{\beta_i} = \kappa_i^3 . \tag{35}$$

The system of model equations (31)-(35) is completed by the normalized modified Rayleigh-Plessset equation (12). Similar to the procedure above for quasi-one-dimensional flows, we eliminate the normalized mixture density $\rho$ and the void fraction $\beta$ using the algebraic relations (31) and (35) in the normalized continuity equation (32), and the normalized pressure field between the normalized modified Rayleigh-Plesset equation (12) and the normalized momentum equations (33) and (34). We then arrive at the following system of evolution equations for the normalized radius R and the normalized velocity field (*u, v*) as

$$\frac{\partial R}{\partial t} = \frac{R^3+\kappa_i^3}{3R^2}\left(\frac{\partial u}{\partial x}+\frac{\partial v}{\partial y}\right) - u\frac{\partial R}{\partial x} - v\frac{\partial R}{\partial y}, \tag{36}$$

$$\frac{\partial u}{\partial t} = a \tag{37}$$

and

$$\frac{\partial v}{\partial t} = b \tag{38}$$

where the unsteady acceleration field ($a$, $b$) satisfies the linear system of integro-partial differential equations

$$\frac{\partial a}{\partial x}+\frac{\partial b}{\partial y} - \frac{R\left[2+(3\Lambda^2-1)\left(R_1/\kappa_i\right)^3\right]}{R_1\left[2+(3\Lambda^2-1)\left(R/\kappa_i\right)^3\right]}\left(\frac{\partial a}{\partial x}+\frac{\partial b}{\partial y}\right)_{y=0}$$
$$-\frac{6R}{L^2\kappa_i^3\left[2+(3\Lambda^2-1)\left(R/\kappa_i\right)^3\right]}\int_0^y \frac{b}{\left[1+\left(R/\kappa_i\right)^3\right]}dy_1 = S_a \tag{39}$$

$$\frac{\partial b}{\partial x}-\frac{\partial a}{\partial y}+\frac{3R^2}{R^3+\kappa_i^3}\left(\frac{\partial R}{\partial y}a-\frac{\partial R}{\partial x}b\right) = S_b \tag{40}$$

where $R_1=R(x,0,t)$ and the source terms $S_a$ and $S_b$ are given by

$$S_a = -\left(u\frac{\partial \psi}{\partial x}+v\frac{\partial \psi}{\partial y}\right)$$
$$+\frac{R\left[2+(3\Lambda^2-1)\left(R_1/\kappa_i\right)^3\right]}{R_1\left[2+(3\Lambda^2-1)\left(R/\kappa_i\right)^3\right]}\left(u\frac{\partial \psi}{\partial x}+v\frac{\partial \psi}{\partial y}\right)_{y=0}$$
$$+\frac{R}{\left[2+(3\Lambda^2-1)\left(R/\kappa_i\right)^3\right]}\int_0^y \mathsf{s}_a\, dy_1 \tag{41}$$

and

$$S_b = -\omega\psi - u\frac{\partial \omega}{\partial x} - v\frac{\partial \omega}{\partial y}$$
$$+\frac{3R^2}{(R^3+\kappa_i^3)}\left[\left(u\frac{\partial v}{\partial x}+v\frac{\partial v}{\partial y}\right)\frac{\partial R}{\partial x}-\left(u\frac{\partial u}{\partial x}+v\frac{\partial u}{\partial y}\right)\frac{\partial R}{\partial y}\right] \tag{42}$$

where $\mathsf{s}_a$ in eq. (41) is defined by

$$\mathsf{s}_a = \frac{6}{L^2\kappa_i^3\left[1+\left(R/\kappa_i\right)^3\right]}\left(u\frac{\partial v}{\partial x}+v\frac{\partial v}{\partial y}\right) + \frac{6}{L^2\kappa_i^3}\frac{\partial p_v}{\partial y}$$
$$-\left\{\frac{2\kappa_i^3\left[(6\Lambda^2-1)\left(R/\kappa_i\right)^6+(6\Lambda^2-2)\left(R/\kappa_i\right)^3-1\right]}{3R^4}\psi\right.$$
$$\left.+\frac{8\left[1+\left(R/\kappa_i\right)^3\right]}{L^2(\mathrm{Re})R^3}\right\}\frac{\partial \psi}{\partial y}$$
$$+\left\{\frac{6S_0}{L^2\kappa_i^3R^2}-\frac{18kp_{g0}}{L^2\kappa_i^3R^{3k+1}}+\frac{24}{L^2(\mathrm{Re})R^4}\psi\right.$$
$$\left.-\frac{2\kappa_i^3\left[(6\Lambda^2-1)\left(R/\kappa_i\right)^6-(3\Lambda^2-1)\left(R/\kappa_i\right)^3+2\right]}{3R^5}\psi^2\right\}\frac{\partial R}{\partial y} \tag{43}$$

In eqs. (41)-(43), $\psi$ and $\omega$, respectively, denote the dilation (in this case the divergence of the velocity field) and the vorticity and are given by

$$\psi = \frac{\partial u}{\partial x}+\frac{\partial v}{\partial y} \tag{44}$$

and

$$\omega = \frac{\partial v}{\partial x}-\frac{\partial u}{\partial y}. \tag{45}$$

Equations (39) and (40) for the unsteady acceleration field ($a$, $b$) constitute the fundamental equations for the transport of the dilation $\psi$ and of the vorticity $\omega$ in 2D bubbly cavitating flows.

In particular, eq. (40) is precisely the non-barotropic vorticity transport equation, called the Fridman equation [10], given by

$$\frac{\partial \boldsymbol{\omega}}{\partial t}+\left(\mathbf{u}.\nabla\right)\boldsymbol{\omega}=-\psi\boldsymbol{\omega}+\left(\boldsymbol{\omega}.\nabla\right)\mathbf{u}+\frac{1}{\rho^2}\nabla\rho\times\nabla p \qquad (46)$$

where the term $\left(\boldsymbol{\omega}.\nabla\right)\mathbf{u}$ vanishes in 2D. Thus it forms the basis for the generation of vorticity in non-barotropic flows and is responsible for the re-entrant jet in partial cavitation and for all closure models of cavitation. *In the absence of cavitation where the source terms* $S_a$ and $S_b$ *vanish, eqs. (39) and (40) reduce to the classical Cauchy-Riemann equations (existence of the complex velocity potential).* The equations for the normalized pressure, normalized density and void fraction then follow from Eqs. (23) and (24) with the dilation now defined by eq. (44).

## THE INITIAL/BOUNDARY VALUE PROBLEMS AND NUMERICAL METHODS OF SOLUTION FOR BUBBLY CAVITATING NOZZLE FLOWS

The quasi-one-dimensional and two-dimensional model equations discussed above for unsteady bubbly cavitating nozzle flows need to be supplemented by appropriate initial and boundary conditions. In what follows we discuss the possible initial and boundary conditions that are suitable for the numerical simulation of the model equations together with the numerical method of solution in each case.

### A. QUASI-ONE-DIMENSIONAL FLOWS

The solution of the hydrodynamic field in unsteady quasi-one-dimensional bubbly cavitating nozzle flows requires the integration of the system of evolution equations (17)-(22) for the bubble radius R and for the flow speed $u$ for a given nozzle geometry (Fig. 1). In this case we first have to specify the initial distributions for the bubble radius and flow speed throughout the whole nozzle, namely

$$R(x,0)=R_0(x) \text{ and } u(x,0)=u_0(x) \text{ for } x_i\le x\le x_e \quad . \qquad (47)$$

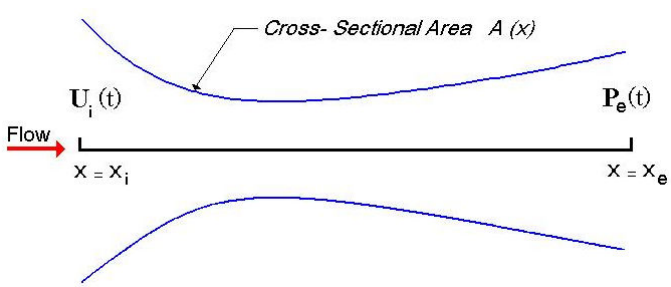


**Figure 1:** Nozzle geometry and boundary conditions for quasi-one-dimensional cavitating nozzle flows.

The initial flow field in this case can be taken as the slightly perturbed steady-state quasi-one-dimensional flow field (for the range of parameters where quasi-one-dimensional steady-state solutions are not possible [6,7], one may start with the incompressible solution supplemented by an everywhere constant bubble radius distribution). To be able to specify the boundary conditions at the nozzle inlet ($x=x_i$) and at the nozzle exit ($x=x_e$), we have to discuss the nature of the evolution equations (17)-(19). In particular, eq. (17) for the bubble radius evolution is hyperbolic for given flow speed so that we need only to specify the bubble radius at the inlet so that

$$R(x_i,t)=R_i(t) \qquad (48)$$

with $R_0(x_i) = R_i(0)$ to avoid a discontinuity in the bubble radius at the nozzle inlet. On the other hand, eqs. (18) and (19) can be combined into a single evolution equation, coupled to the flow speed and bubble radius, as

$$\frac{\partial u}{\partial t}=a(x,t)=K_1(t)\mathcal{A}_1(x,t)+K_2(t)\mathcal{A}_2(x,t)$$

$$+\mathcal{A}_2(x,t)\int_{x_i}^{x}\frac{\left[\overline{s}(\xi,t)\mathcal{A}_1(\xi,t)+u\ (\partial^2u/\partial\xi^2)(\partial\mathcal{A}_1/\partial\xi)\right]}{W(\xi,t)}d\xi$$

$$-\mathcal{A}_1(x,t)\int_{x_i}^{x}\frac{\left[\overline{s}(\xi,t)\mathcal{A}_2(\xi,t)+u\ (\partial^2u/\partial\xi^2)(\partial\mathcal{A}_2/\partial\xi)\right]}{W(\xi,t)}d\xi \qquad (49)$$

where $W$ represents the Wronskian of the two linearly independent solutions $\mathcal{A}_1$ and $\mathcal{A}_2$ of the linear homogeneous equation corresponding to eq. (19) for the unsteady acceleration $a$ and is given by

$$W(x,t)=\mathcal{A}_1\frac{\partial\mathcal{A}_2}{\partial x}-\mathcal{A}_2\frac{\partial\mathcal{A}_1}{\partial x} \quad , \qquad (50)$$

and where $K_1(t)$ and $K_2(t)$ are time dependent functions to be determined from the nozzle inlet and exit boundary conditions and $\overline{s}$ is given by

$$\overline{s}(x,t)=\overline{s}(R,u,\frac{\partial R}{\partial x},\frac{\partial u}{\partial x},\frac{\partial^2 u}{\partial x^2},x)$$

$$=s(R,u,\frac{\partial R}{\partial x},\frac{\partial u}{\partial x},\frac{\partial^2 u}{\partial x^2},\frac{\partial^3 u}{\partial x^3},x)+u\frac{\partial^3 u}{\partial x^3}+\frac{\partial^2 u}{\partial x^2}[\frac{\partial u}{\partial x}+u\ g(R,\frac{\partial R}{\partial x},x)]$$

$$=-\left\{\left[\left(\frac{F_4(R)}{F_2(R)}-1\right)\left(\frac{\partial u}{\partial x}+\frac{u}{A}\frac{dA}{dx}\right)+\frac{F_5(R)}{F_2(R)}\right]\frac{\partial^2 u}{\partial x^2}\right.$$

$$+\frac{F_6(R)}{F_2(R)}\frac{\partial R}{\partial x}\left(\frac{\partial u}{\partial x}\right)^2+\left[\frac{F_7(R)}{F_2(R)}u\left(\frac{1}{A}\frac{dA}{dx}\right)-3\frac{F_3(R)F_5(R)}{RF_2(R)}\right]\frac{\partial R}{\partial x}\frac{\partial u}{\partial x}$$

$$+\frac{F_4(R)}{F_2(R)}\left(\frac{1}{A}\frac{dA}{dx}\right)\left(\frac{\partial u}{\partial x}\right)^2+\left[\frac{F_8(R)}{F_2(R)}u\frac{d}{dx}\left(\frac{1}{A}\frac{dA}{dx}\right)\right.$$

$$\left.+\frac{F_9(R)}{F_2(R)}u\left(\frac{1}{A}\frac{dA}{dx}\right)^2+\frac{F_5(R)}{F_2(R)}\left(\frac{1}{A}\frac{dA}{dx}\right)+\frac{F_3(R)}{F_2(R)}u\right]\frac{\partial u}{\partial x}$$

$$+\left[\frac{F_6(R)}{F_2(R)}u^2\left(\frac{1}{A}\frac{dA}{dx}\right)^2-3\frac{F_3(R)F_5(R)}{RF_2(R)}u\left(\frac{1}{A}\frac{dA}{dx}\right)\right.$$

$$\left.+\frac{F_1(R)}{F_2(R)}u^2\frac{d}{dx}\left(\frac{1}{A}\frac{dA}{dx}\right)+\frac{F_{10}(R)}{F_2(R)}\right]\frac{\partial R}{\partial x}$$

$$+\frac{F_9(R)}{F_2(R)}u^2\left(\frac{1}{A}\frac{dA}{dx}\right)\frac{d}{dx}\left(\frac{1}{A}\frac{dA}{dx}\right)+u^2\frac{d^2}{dx^2}\left(\frac{1}{A}\frac{dA}{dx}\right)$$

$$\left.+\frac{F_5(R)}{F_2(R)}u\frac{d}{dx}\left(\frac{1}{A}\frac{dA}{dx}\right)+\frac{\partial p_v/\partial x}{F_2(R)}\right\}\quad . \tag{51}$$

In order to evaluate the time dependent functions $K_1(t)$ and $K_2(t)$ in eq. (49), we consider the appropriate boundary conditions at the inlet and outlet of the nozzle. For real cavitating flows, either of the following two sets of boundary conditions can be specified:

*(a) The inlet flow speed and exit pressure are specified*, i.e.

$$u(x_i,t)=U_i(t) \text{ and } p(x_e,t)=P_e(t) \text{ for } t\geq 0 \tag{52}$$

together with $U_i(0)=u_0(x_i)$ and $P_e(0)=p(x_e,0)$ to ensure continuity of the solutions.

*(b) The inlet and exit pressures are specified*, i.e.

$$p(x_i,t)=P_i(t) \text{ and } p(x_e,t)=P_e(t) \text{ for } t\geq 0 \tag{53}$$

together with $P_i(0)= p(x_i,0)$ and $P_e(0)=p(x_e,0)$ to ensure continuity of the solutions.

The evaluation of the time dependent functions $K_1(t)$ and $K_2(t)$ in eq. (49) corresponding to the boundary conditions in each case are given in appendix B. It should be mentioned that the boundary conditions of case (b) require enormous amount of computation time. Therefore, for simplicity, we adopt the boundary conditions of case (a).

For the numerical method, we first evaluate the unsteady acceleration field by eq. (49) at every instant $t$ using the flow speed distribution $u(x,t)$ and the radius distribution $R(x,t)$ at that instant, starting with the initial distributions $u_0(x)$ and $R_0(x)$. The homogeneous solutions $\mathcal{A}_1$ and $\mathcal{A}_2$ of eq. (19) for the unsteady acceleration are obtained by power series methods of second order linear ordinary differential equations with variable coefficients. The time dependent functions $K_1(t)$ and $K_2(t)$ are evaluated using non-reflecting boundary conditions. Using the unsteady acceleration field, the evolution eq. (18) is integrated using a multi-stage Runge-Kutta method in time to arrive at the flow speed distribution at the next time step. Using the flow speed thus obtained, the first order hyperbolic equation (17) for the bubble radius R is integrated by the classical method of characteristics. Thus the solutions for the flow speed and radius distributions of the evolution equations are obtained for the next time step. The procedure is repeated in a similar manner for all subsequent time steps.

### B. TWO-DIMENSIONAL FLOWS

In order to discuss the solution of the two-dimensional system of evolution equations (36)-(45) of the bubble radius and flow velocity field for cavitating nozzle flows, they should be supplemented by appropriate initial bubble radius and velocity field distributions together with inlet and exit boundary conditions, similar to the case discussed for quasi-one-dimensional flows. In this case the length of the quasi-1D nozzle is elongated in both the inlet and exit directions with corresponding constant inlet and exit areas to ensure uniform inlet and exit boundary conditions across the cross-sectional area at the inlet and exit of the nozzle, as shown in Fig. 2. We also assume a symmetric configuration of the flow field in the y-direction so that it is also sufficient to discuss the solution in the upper symmetric domain of the nozzle. In specifying the initial distributions of the bubble radius and velocity field for the evolution equations, care should be taken to start with irrotational flow in order to access the correct order of magnitude of vorticity generated in the cavitating regime. Therefore, we choose the initial flow field

$$u(x,y,0)=u_0(x,y) \text{ and } v(x,y,0)=v_0(x,y) \tag{54}$$

to be irrotational everywhere in the computational domain and uniform and uni-directional ($v$=0) at the nozzle inlet and exit (i.e., at $x=x_i$ and $x=x_e$) . We also take the initial radius distribution

$$R(x,y,0)=R_0(x,y) \tag{55}$$

in such a way that it is also uniform at the nozzle inlet and exit. Taking into account the hyperbolicity of eq. (36) for the bubble radius for given velocity field, we need only to specify the bubble radius at the inlet. Assuming that the inlet bubble radius distribution is uniform in y at all times, we have

$$R(x_i,y,t)=R_i(t) \tag{56}$$

with $R_i(0)$ being equal to the corresponding initial inlet bubble radius to avoid a discontinuity in the bubble radius at the nozzle inlet. Similar to the procedure of quasi-1D flows, we can specify two sets of boundary conditions:

*(a) The inlet flow speed and exit pressure, both uniform, are specified*, i.e.

$$u(x_i, y, t) = U_i(t)\,,\ v(x_i, y, t) = 0 \quad \text{and} \quad p(x_e, y, t) = P_e(t) \tag{57}$$

for t≥0 together with $U_i(0)$ and $P_e(0)$ matching the corresponding initial inlet and exit values to ensure continuity of the solutions.

*(b) The uniform inlet and exit pressures are specified* , i.e.

$$p(x_i, y, t) = P_i(t) \quad \text{and} \quad p(x_e, y, t) = P_e(t) \tag{58}$$

for t≥0 together with $P_i(0)$ and $P_e(0)$ matching the corresponding initial inlet and exit values to ensure continuity of the solutions.

The above boundary conditions, similar to the procedure in quasi-one-dimensional flows, should be converted to the boundary conditions for the unsteady acceleration field for the integro-partial differential system, given by eqs. (39) and (40). For this reason, assuming that the inlet velocity field is uniform and unidirectional and that the bubbles are in mechanical equilibrium at the inlet and exit of the nozzle and using eq. (23) for the pressure field, we can arrive at the following boundary conditions for the system of eqs. (39) and (40) in each case :

*Case (a) The inlet flow speed and exit pressure, both uniform, are specified.*

$$a = 0 \ \text{and}\ b{=}0 \ \text{at}\ x = x_i\ ,\ a_x = 0 \ \text{and}\ b{=}0 \ \text{at}\ x = x_e\ ,$$

$$a_y = 0 \ \text{and}\ b{=}0 \ \text{at}\ y = 0,\ b = a\tan\theta \ \text{at}\ \text{y = h(x)} \tag{59}$$

where $y=h(x)$ denotes the shape of the upper wall of the nozzle and $\tan\theta = dh/dx$. Such a configuration of the boundary conditions are given in Fig. 2.

*Case (b) The uniform inlet and exit pressures are specified.*

$$a_x = 0 \ \text{and}\ b{=}0 \ \text{at}\ x = x_i\ ,\ a_x = 0 \ \text{and}\ b{=}0 \ \text{at}\ x = x_e\ ,$$

$$a_y = 0 \ \text{and}\ b{=}0 \ \text{at}\ y = 0,\ b = a\tan\theta \ \text{at}\ y = h(x). \tag{60}$$

For the numerical method, similar to the procedure for quasi-1D flows, we first consider the integro-partial differential system of equations, given by eqs. (39) and (40), subject to boundary conditions given by either eq. (59) or eq. (60). The system is solved in two iterative steps. In the first step the integral on the left-hand side of eq. (39) is set equal to zero and the remaining elliptic system of first order partial differential equations is first discretized by a central finite difference scheme. The resulting linear system of algebraic equations, subject to the boundary conditions given in eq. (59) or in eq. (60), are solved by Gauss-Seidel Over Relaxation Method. In the second step, the skipped integral on the left hand side of eq. (39) is evaluated and treated as a source term. The first step is then repeated to obtain the unsteady acceleration field at that instant. Using a multi-stage Runge-Kutta method in time and the solution for the unsteady acceleration field, the evolution eqs. (37) and (38) are integrated to yield the velocity field in the next step. Using this velocity field, the hyperbolic evolution equation (36) is integrated by the method of characteristics or by using flux splitting methods to arrive at the bubble radius in the next time step. The numerical scheme is then to be repeated for all subsequent time steps.

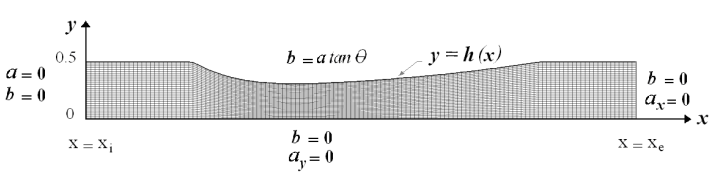


**Figure 2:** Nozzle geometry and boundary conditions of the unsteady acceleration field for two-dimensional cavitating nozzle flows.

## AN EQUILIBRIUM PHASE TRANSITION MODEL: CATUM

In this section we discuss an equilibrium phase transition model by Schnerr et al. [11-14], which is particularly useful in describing wave dynamics in cavitating flows. Although this model by-passes the details of bubble dynamics, it still can prove useful, particularly, in describing wave dynamics related to the collapse of bubble clouds. Since bubble nucleation in cavitating flows occur by heterogeneous nucleation, the initial phase change occurs near thermodynamic equilibrium. It is also known that bubble growth occurs almost isothermally with small temperature variations so that the increase in void fraction of the two-phase mixture can be accessed by this small variation in temperature regarding the compressibility of the two-phase mixture, leaving out all the detailed phenomena arising from bubble dynamics. In this model, called CATUM by its originators, a two-phase homogeneous mixture model is assumed where, similar to homogeneous bubbly flows, the single phase flow equations apply. In contrast to the change of the homogeneous mixture properties by cooperative dynamics of the bubbles, in CATUM the homogeneous mixture properties are defined by the internal energy and the density of the mixture. More precisely, the mixture density $\rho'$, the mixture pressure $p'$ and the mixture internal energy $e'$ at the mixture temperature $T'$ at thermodynamic equilibrium are given by

$$\rho' = (1-\beta)\ \rho_{\ell sat}{}'(T') + \beta\,\rho_{vsat}{}'(T')\ , \tag{61}$$

$$\rho' e' = (1-\beta)\ \rho_{\ell sat}{}'(T') + \beta\,\rho_{vsat}{}'(T')\,e_v'(T') \tag{62}$$

and

$$p' = p_{sat}{}'(T') \tag{63}$$

where the subscripts $\ell$, $v$ and $sat$ refer, respectively, to pure liquid, vapor and saturated states. The pure vapor state ($\beta=1$) is described by perfect gas relations and the pure liquid ($\beta=0$) equation of state is described by a modified Tait law as

$$\frac{p' + B'}{p_{sat}{}'(T') + B'} = \left(\frac{\rho'}{\rho_{sat}{}'(T')}\right)^N \tag{64}$$

where $B'$ and $N$ are constants. Equations (61)-(64) together with the classical continuity, Euler momentum and energy equations form the basic model equations of CATUM. In particular, eqs. (61) and (62) for the two-phase mixture are solved for the mixture temperature $T'$ and for the void fraction $\beta$. The mixture pressure is then determined by the Clausius-Clapeyron relation, eq. (63).

Since the Euler equations can be expressed in the form of conservation laws, it is self-evident that the numerical method of CATUM is based on a cell centered finite volume formulation of conserved quantities. The resulting semi-discrete equations are then integrated in time using a second order explicit multistage Runge-Kutta method. The spatial discretization heavily relies on approximate Riemann solvers (Godunov-type schemes [28]). These methods have the advantage of capturing waves, of even high frequency, very accurately. Their drawback is the low Mach number limit. To overcome this difficulty, a Riemann solver to determine the mass flow together with a modified pressure flux that is consistent for low and high Mach number flow is developed [12]. The application of the numerical scheme to flows with phase change requires considerable attention, particularly during the last stages of condensation where the sonic speed rapidly increases in order of magnitudes. Here a modification based on the dissipative formulation of the numerical flux function is made. In this way the developed CFD-Tool CATUM enables capturing wave propagation properties from very low Mach numbers to appreciable Mach numbers. As for the treatment of the boundaries, a ghost-cell based approach is used. A physical wall boundary is assumed to be impermeable, adiabatic and inviscid, the flow tangency condition being achieved by mirroring the normal velocity component. Weakly reflecting boundary conditions are adopted at the inlet and the outlet of the numerical domain. Details of the numerical model, its implementation and its validation are given in [11-14].

## RESULTS AND DISCUSSION

We now consider the quasi-one-dimensional and two-dimensional cavitating flows whose geometric configuration is shown in Fig. 3 (for quasi-one-dimensional flows, the inlet and exit of the nozzle are taken as shown in Fig.1 so that the specified exit pressure matches the measured value at the wall).

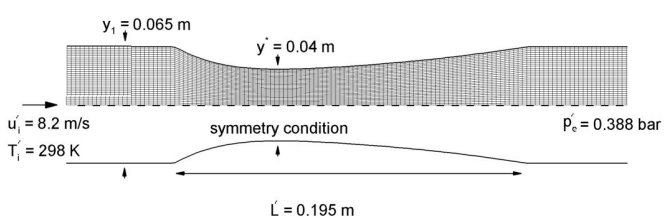


**Figure 3:** 2D plane computational domain and boundary conditions (symmetry boundary condition enforces flow symmetry).

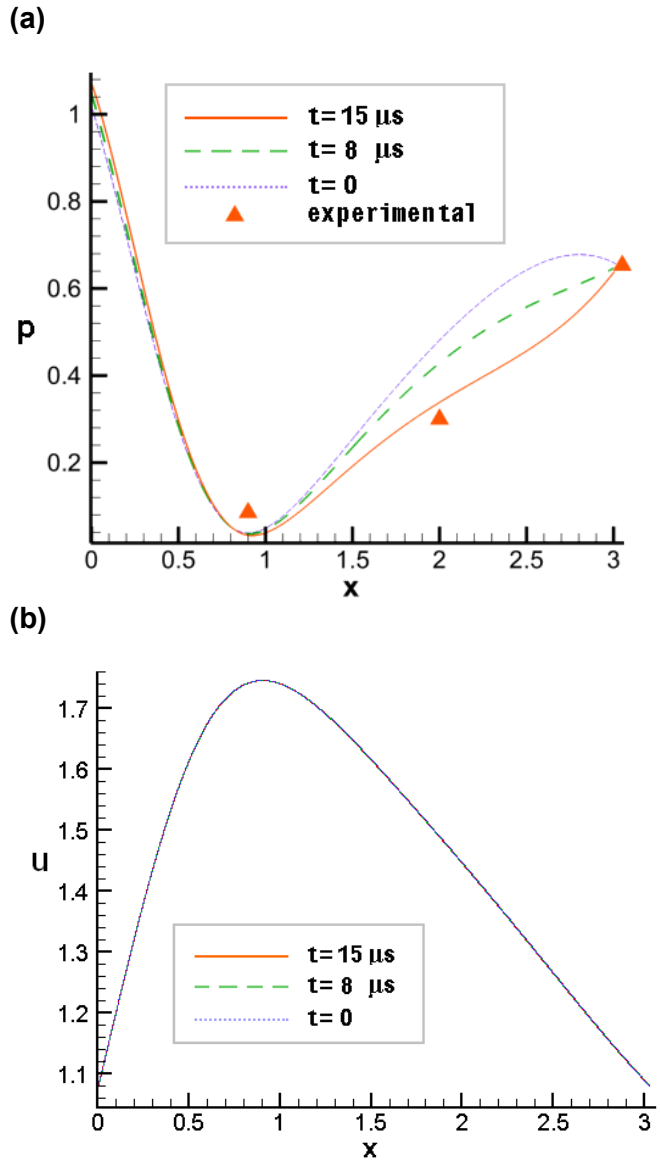


**Figure 4:** The unsteady quasi-1D distributions of **(a)** the pressure and **(b)** the flow speed at three instants of time for the cavitating nozzle flow of water with air bubbles with initial inlet void fraction $\beta_{i0} = 10^{-6}$, initial inlet bubble radius $R'_{i0}$=50 µm, inlet flow speed $u'_i$ = 8.2 m/s and exit pressure $p'_e$ = 0.388 bar ( the experimental results shown above for the pressure are the mean pressure measurements over a cycle, they fluctuate within ±2.0 kPa).

For quasi-one-dimensional flows, we present results for the bubbly liquid mixture model whereas, for two-dimensional flows, we present results only for the equilibrium phase transition model since an accurate 2D algorithm for bubbly cavitating flows along the numerical procedure outlined above is under construction and the results for the bubbly mixture model are not yet available. Therefore, a quantitative comparison of the results of the models can not be given at this stage. The only quantitative comparison we will present will be the comparison of the pressure distribution obtained for quasi-

one-dimensional bubbly cavitating nozzle flows against the measured pressure values at the wall of the nozzle under the experimental conditions.

For quasi-one-dimensional flows, we consider the two-phase dispersed flow of water with air bubbles with time –averaged inlet flow speed $u'_i$ =8.2 m/s , initial inlet void fraction $\beta_{i0}$ = $10^{-6}$, initial inlet bubble radius $R'_{i0}$ =50 μm and time-averaged exit pressure $p'_e$ = 0.388 bar. For the initial field we use a slightly perturbed steady-state distribution for the bubble radius and flow speed. Under the stated conditions, the steady-state solution shows that the bubbles grow slightly reaching their maximum size and then they return to their initial size, as also shown in Fig. 5(a) [29]. In this case the large growth and violent collapse of the bubbles do not occur and the bubbles seem to be in local mechanical equilibrium. To reach unsteady cavitating flow conditions, we lower the exit pressure until the specified exit pressure under the unsteady cavitating flow conditions is reached. The normalized pressure, normalized flow speed, normalized bubble radius and normalized unsteady acceleration distributions along the nozzle axis obtained by the bubbly flow model are shown in Figs. 4 and 5 at three instants of time at the start of unsteady cavitation. In these figures the transient distributions are ignored and the time $t=0$ is artificially set at the begining of unsteady cavitation. It is seen in Fig. 4(a) that reasonable agreement is achieved between the quasi-one-dimensional unsteady pressure distributions and the measured values from the experiments performed at the Mechanical Engineering Department at Istanbul Technical University under the same conditions. On the other hand, a close examination of the unsteady distributions in Figs. 3 and 4 show that the flow speed and the bubble radius distributions (consequently, the density and void fraction distributions) seem to deviate only slightly fom the initially specified slightly perturbed steady-state distributions, since the cavitation sheets attached to the nozzle walls, in this case, have small thicknesses compared to the nozzle height, thus influencing these distributions only slightly. However, the presence of unsteady cavitation leads to pressure losses which are accommodated by large values of the unsteady acceleration. These large values of the unsteady acceleration are balanced by the pressure gradients. They do not contribute to the flow speed significantly because of the very small characteristic times involved.

The two-dimensional results under the same experimental conditions (uniform inlet speed $u'_i$ = 8.2 m/s and uniform exit pressure $p'_e$ = 0.388 bar) are numerically simulated by the equilibrium phase transition model using the code CATUM. A symmetry boundary condition is imposed so that the upper half of the nozzle is chosen to be the computational domain. This ensures flow symmetry, *a priori*. The liquid inflow is assumed

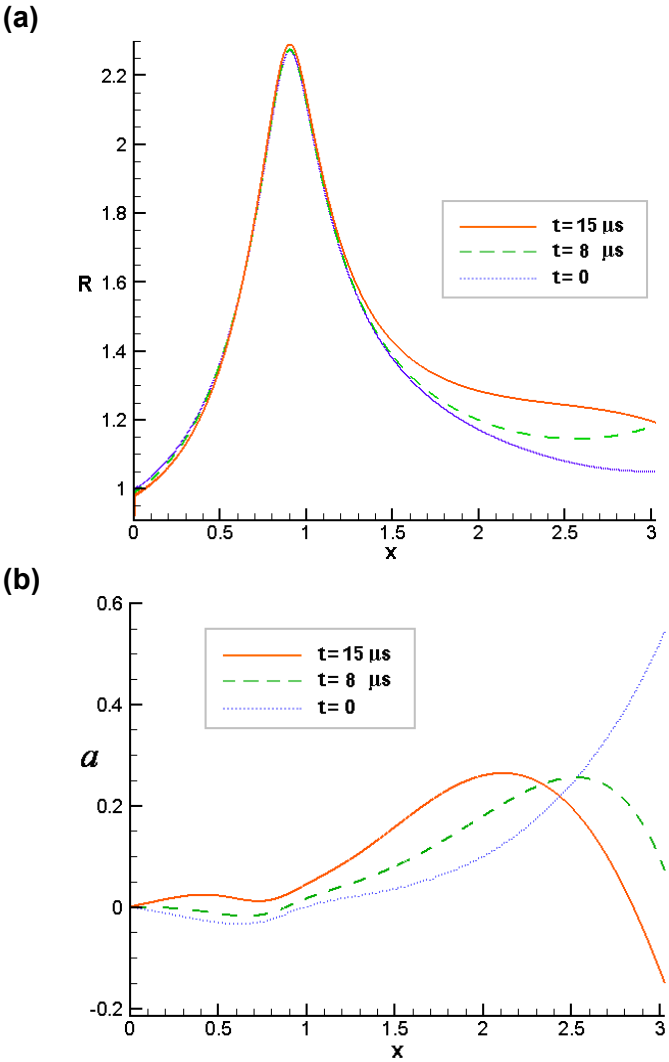


**Figure 5:** The unsteady quasi-1D distributions of **(a)** bubble radius and **(b)** unsteady acceleration at three instants of time for the cavitating nozzle flow of water with air bubbles with inlet void fraction $\beta_{i0}$ = $10^{-6}$, inlet bubble radius $R'_{i0}$=50 μm, inlet flow speed $u'_i$ = 8.2 m/s and exit pressure $p'_e$ = 0.388 bar.

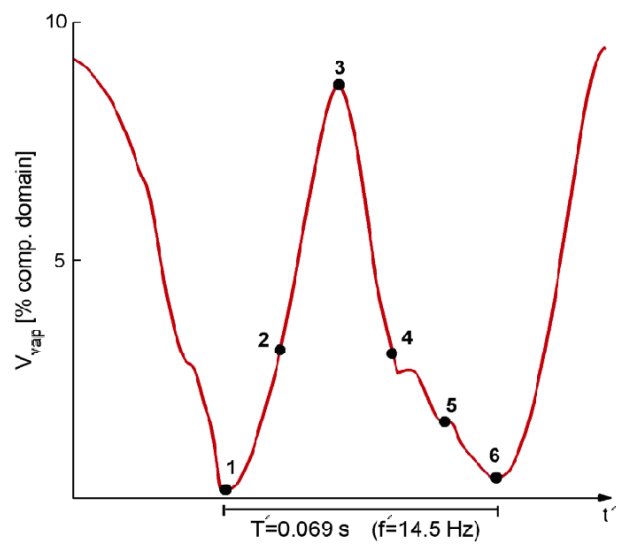


**Figure 6:** Time evolution of the total vapor volume [% comp. domain], a typical cycle of six equidistant instants of time 1 to 6 with shedding frequency f' ≈ 14.5 Hz and period T'=0.069 s.

to be pure water at the temperature 298 K. The simulation is performed on the nozzle grid shown in detail in Fig. 3 using 4000 cells. A second order accurate numerical scheme is used both in space and time. The results for the total volume percentage of the vapor formed by cavitation is plotted against real time in Fig. 6 where a typical cavitation pattern with shedding frequency $f'$=14.5 Hz (corresponding to a cycle period of 0.069 s) is identified at 6 time instants. The maximum volume percentage with respect to the computational domain is about 9% and occurs at time instant 3. The length of the of 0.069 s) is identified at 6 time instants. The maximum attached cavity is calculated as 0.126m. The distributions of the void fraction at six instances of time are shown in Fig. 7. A sheet cavity is developed at instant 3 on both sides of the wall, followed by a re-entrant jet at instant 4 followed by cloud shedding at instant 5 and finally the collapse of the cloud at instant 6, typical of a partial cavitation cycle. The results for the

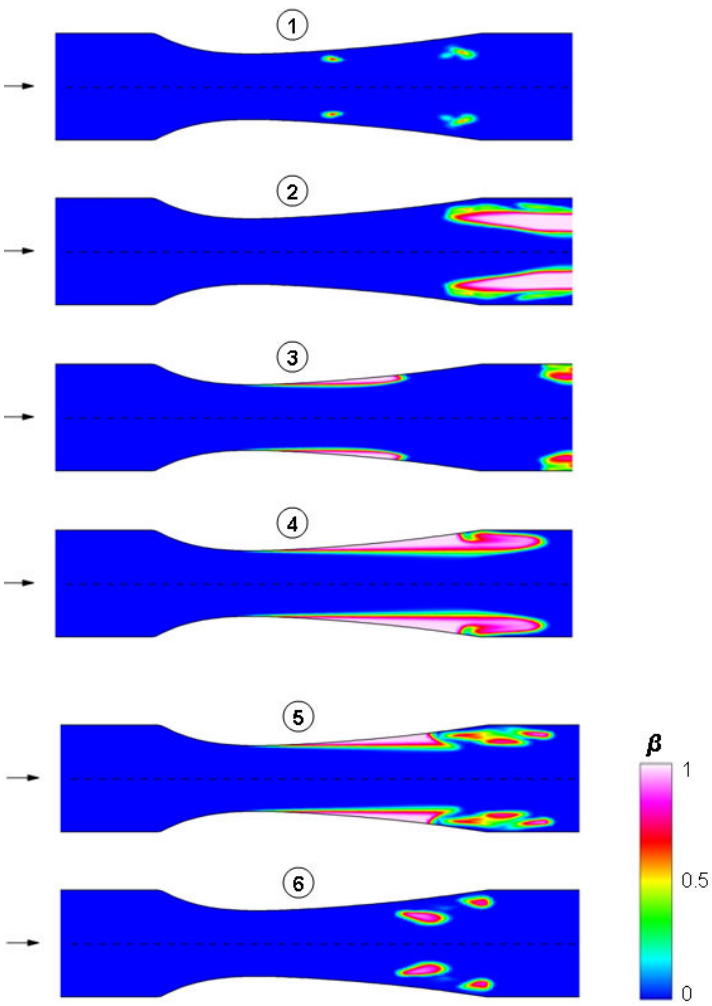


**Figure 7:** Vapor volume fraction $\beta$ at six instants of time (enforced flow symmetry due to symmetry boundary condition). Shedding frequency f′ ≈ 14.5 Hz, period T′=0.069 s.

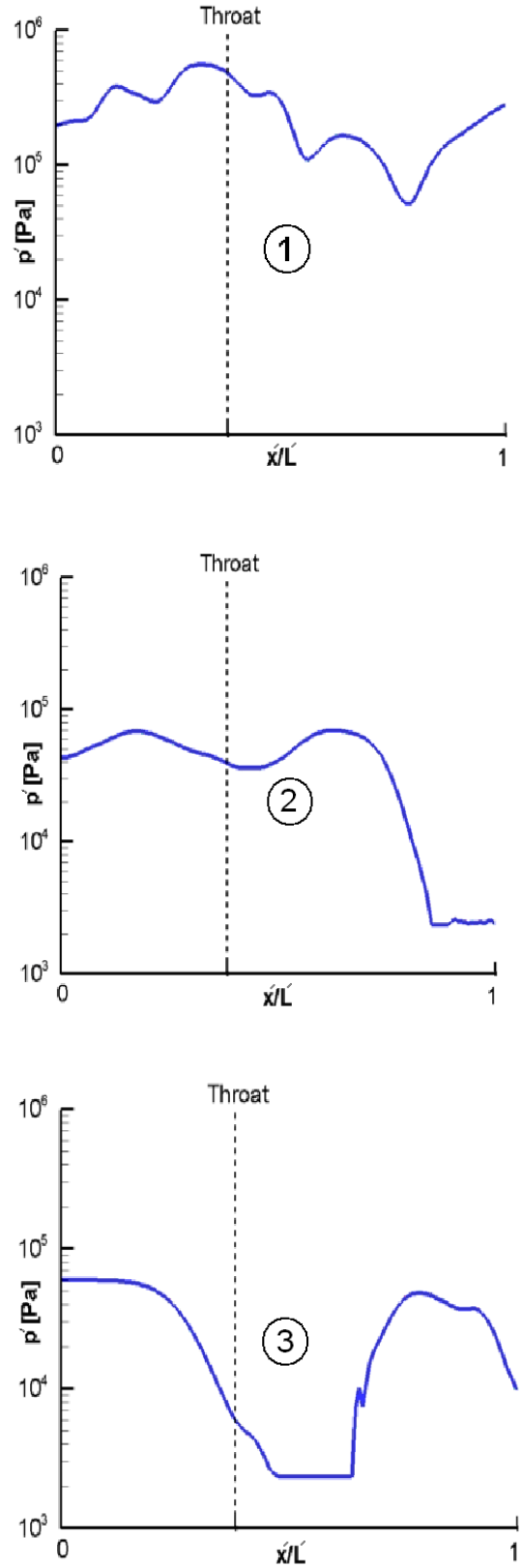


**Figure 8:** Static pressure distribution along the nozzle axis corresponding to time instants 1, 2 and 3 in Figure 6.

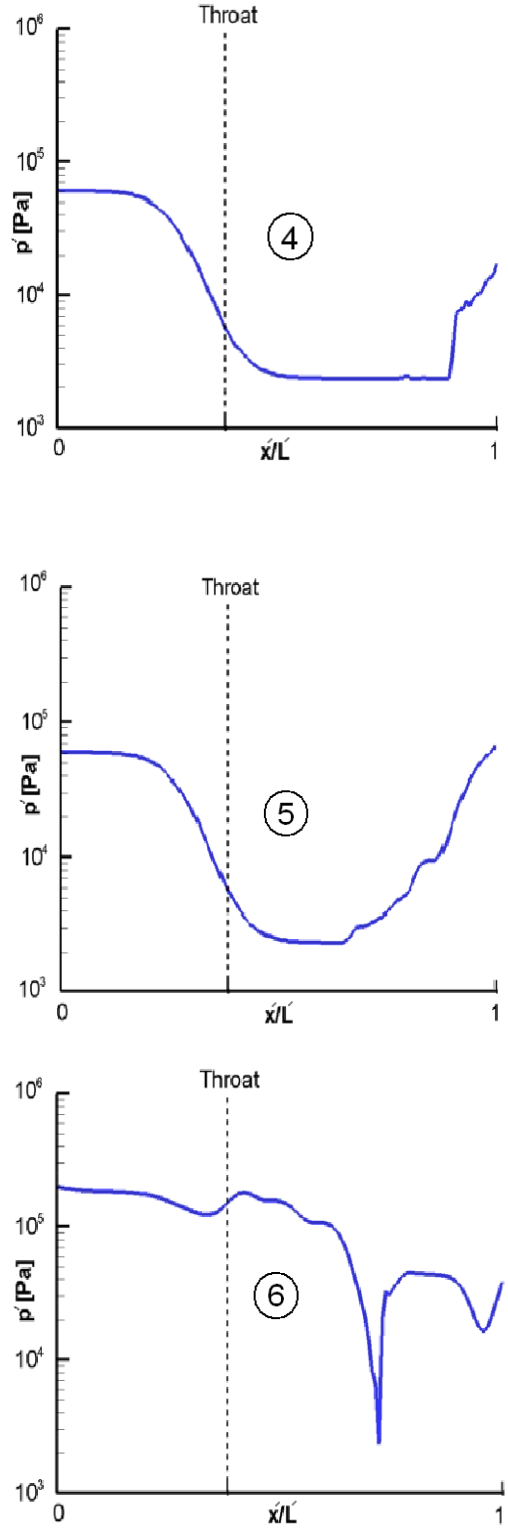


**Figure 9:** Static pressure distribution along the nozzle axis corresponding to time instant 4, 5 and 6 in Figure 6.

static pressure distributions along the nozzle axis at six instances of time are shown in Figs. 8 and 9. The high pressures attained at time instances 1 and 6 are instantaneous pulses due to the collapse of the clouds. In other time instances the static pressure distributions are of the same order of magnitude of the measured static pressures at the wall. In this case a direct comparison with the static pressure distributions with those of the quasi-one-dimensional bubbly flow model is not possible due to the two-dimensional structure of the attached cavities and of cloud shedding.

## CONCLUSIONS

Model equations for quasi-one-dimensional and two-dimensional bubbly cavitating nozzle flows are presented and the evolution equations for the bubble radius and velocity field in each case are obtained. In particular, in two-dimensional flows the integro-partial differential system of equations for the unsteady acceleration field, which enters the evolution equations for the velocity field, is shown to constitute the fundamental equations of 2D cavitating flows, exhibiting the evolution of the dilation and of the vorticity. The initial/boundary value problems are then formulated for both unsteady quasi-one-dimensional and two-dimensional bubbly cavitating nozzle flows. Results obtained for the unsteady quasi-one-dimensional case show that it is possible to determine the pressure loss due to cavitation in this case. However, the quasi-one-dimensional model is insufficient in describing the two-dimensional flow structures. Since an algorithm to calculate the unsteady 2D bubbly flow model is yet not available, the 2D results were calculated by the CATUM algorithm based on an equilibrium phase transition model. The 2D results show considerable rise in pressure at instants of bubble collapse in the entire model. A 2D algorithm for the numerical simulation of bubbly cavitating nozzle flows, as summarized in this paper, is under construction and the results will be compared with those presented here by the CATUM algorithm. Such a comparison will be useful in quantifying the order of magnitude of the pressure values achieved during a cavitation cycle.

## ACKNOWLEDGMENTS

This work has in part been supported by TÜBİTAK under project number 105M035 and in part by Deutsche Forschungs-gemeinschaft (DFG) contract SCHN 352/24-1.

## APPENDIX A:

The functions $F_j\,(R)$ ; $j$=1,2,...,10 entering eqs. (20)-(22) are

$$F_1(R) = -\frac{L^2\kappa_i^3}{3R^2\left[1+\left(R/\kappa_i\right)^3\right]}$$

$$\times\left[\left(3\Lambda^2-1\right)\left(R/\kappa_i\right)^6+\left(3\Lambda^2-2\right)\left(R/\kappa_i\right)^3-1\right], \qquad \text{(A1)}$$

$$F_2(R) = -\frac{L^2\kappa_i^3}{6R}\left[2+\left(3\Lambda^2-1\right)\left(R/\kappa_i\right)^3\right], \tag{A2}$$

$$F_3(R) = \frac{1}{\left[1+\left(R/\kappa_i\right)^3\right]}, \tag{A3}$$

$$F_4(R) = -\frac{L^2\kappa_i^6}{18R^4}\left[\left(21\Lambda^2-5\right)\left(R/\kappa_i\right)^6 + \left(12\Lambda^2+2\right)\left(R/\kappa_i\right)^3-2\right], \tag{A4}$$

$$F_5(R) = -\frac{4\kappa_i^3}{3(\mathrm{Re})R^3}\left[1+\left(R/\kappa_i\right)^3\right], \tag{A5}$$

$$F_6(R) = -\frac{L^2\kappa_i^6}{18R^5\left[1+\left(R/\kappa_i\right)^3\right]}\left[\left(12\Lambda^2-2\right)\left(R/\kappa_i\right)^9 + 6\Lambda^2\left(R/\kappa_i\right)^6 - 6\left(\Lambda^2-1\right)\left(R/\kappa_i\right)^3+4\right], \tag{A6}$$

$$F_7(R) = -\frac{L^2\kappa_i^6}{9R^5\left[1+\left(R/\kappa_i\right)^3\right]}\left[\left(21\Lambda^2-5\right)\left(R/\kappa_i\right)^9 + \left(15\Lambda^2-6\right)\left(R/\kappa_i\right)^6 + \left(-6\Lambda^2+3\right)\left(R/\kappa_i\right)^3+4\right], \tag{A7}$$

$$F_8(R) = -\frac{L^2\kappa_i^6}{18R^4}\left[\left(39\Lambda^2-11\right)\left(R/\kappa_i\right)^6 + \left(12\Lambda^2+14\right)\left(R/\kappa_i\right)^3-2\right], \tag{A8}$$

$$F_9(R) = -\frac{L^2\kappa_i^6}{18R^4}\left[\left(12\Lambda^2-2\right)\left(R/\kappa_i\right)^6 + \left(12\Lambda^2-4\right)\left(R/\kappa_i\right)^3-2\right], \tag{A9}$$

$$F_{10}(R) = \frac{S_0}{R^2} - \frac{3kP_{g_i}}{R^{3k+1}}. \tag{A10}$$

## APPENDIX B:

The boundary conditions presented for the cases (a) and (b) in quasi-one-dimensional flows should be converted to the boundary conditions for the unsteady acceleration field in order to pose a two-point boundary value problem for the unsteady acceleration field given by eq. (19). For this reason, using eq. (23) for the pressure distribution in quasi-one-dimensional flows, we can arrive at the boundary conditions for the unsteady acceleration field corresponding to the inlet and exit pressure boundary conditions as

$$\left(\frac{\partial a}{\partial x}\right)_i + \left(\frac{1}{A}\frac{dA}{dx}\right)_i a_i = Q_i(t) \tag{B1}$$

and

$$\left(\frac{\partial a}{\partial x}\right)_e + \left(\frac{1}{A}\frac{dA}{dx}\right)_e a_e = Q_e(t) - \left[\left(\frac{\partial \mathcal{A}_1}{\partial x}\right)_e + \left(\frac{1}{A}\frac{dA}{dx}\right)_e (\mathcal{A}_1)_e\right] \times \int_{x_i}^{x_e} \frac{\left[\overline{s}(\xi,t)\mathcal{A}_2(\xi,t) + u\ (\partial^2 u/\partial\xi^2)(\partial\mathcal{A}_2/\partial\xi)\right]}{W(\xi,t)} d\xi$$

$$+\left[\left(\frac{\partial \mathcal{A}_2}{\partial x}\right)_e + \left(\frac{1}{A}\frac{dA}{dx}\right)_e (\mathcal{A}_2)_e\right] \times \int_{x_i}^{x_e} \frac{\left[\overline{s}(\xi,t)\mathcal{A}_1(\xi,t) + u\ (\partial^2 u/\partial\xi^2)(\partial\mathcal{A}_1/\partial\xi)\right]}{W(\xi,t)} d\xi \tag{B2}$$

where the functions $Q_i(t)$ and $Q_e(t)$ are defined by

$$Q_i(t) = -U_i\left\{\left(\frac{1}{A}\frac{dA}{dx}\right)_i\left(\frac{\partial u}{\partial x}\right)_i + U_i\left[\frac{d}{dx}\left(\frac{1}{A}\frac{dA}{dx}\right)\right]_i\right\}$$
$$-\frac{\kappa_i^3\left[(6\Lambda^2-1)(R_i/\kappa_i)^6 + (6\Lambda^2-2)(R_i/\kappa_i)^3-1\right]}{3R_i^3\left[2+(3\Lambda^2-1)(R_i/\kappa_i)^3\right]} \times \left[\left(\frac{1}{A}\frac{dA}{dx}\right)_i U_i + \left(\frac{\partial u}{\partial x}\right)_i\right]^2$$
$$+\frac{6R_i}{L^2\kappa_i^3\left[2+(3\Lambda^2-1)(R_i/\kappa_i)^3\right]}\left[(p_v)_i - \frac{S_0}{R_i} + \frac{p_{gi}}{R_i^{3k}} - P_i\right]$$
$$-\frac{8\left[1+\left(R_i/\kappa_i\right)^3\right]}{L^2(\mathrm{Re})R_i^2\left[2+(3\Lambda^2-1)(R_i/\kappa_i)^3\right]}\left[\left(\frac{1}{A}\frac{dA}{dx}\right)_i U_i + \left(\frac{\partial u}{\partial x}\right)_i\right] \tag{B3}$$

$$Q_e(t) = -U_e\left\{\left(\frac{1}{A}\frac{dA}{dx}\right)_e\left(\frac{\partial u}{\partial x}\right)_e + U_e\left[\frac{d}{dx}\left(\frac{1}{A}\frac{dA}{dx}\right)\right]_e\right\}$$
$$-\frac{\kappa_i^3\left[(6\Lambda^2-1)(R_e/\kappa_i)^6 + (6\Lambda^2-2)(R_e/\kappa_i)^3-1\right]}{3R_e^3\left[2+(3\Lambda^2-1)(R_e/\kappa_i)^3\right]} \times \left[\left(\frac{1}{A}\frac{dA}{dx}\right)_e U_e + \left(\frac{\partial u}{\partial x}\right)_e\right]^2$$

$$+\frac{6R_e}{L^2\kappa_i^3\left[2+(3\Lambda^2-1)(R_e/\kappa_i)^3\right]}\left[(p_v)_e-\frac{S_0}{R_e}+\frac{p_{gi}}{R_e^{3k}}-P_e\right]$$

$$-\frac{8\left[1+\left(R_e/\kappa_i\right)^3\right]}{L^2(\mathrm{Re})R_e^2\left[2+(3\Lambda^2-1)(R_e/\kappa_i)^3\right]}\left[\left(\frac{1}{A}\frac{dA}{dx}\right)_e U_e+\left(\frac{\partial u}{\partial x}\right)_e\right]$$

$$+\left[\left(\frac{\partial \mathcal{A}_1}{\partial x}\right)_e+\left(\frac{1}{A}\frac{dA}{dx}\right)_e(\mathcal{A}_1)_e\right]$$
$$\times\int_{x_i}^{x_e}\frac{\left[\overline{s}(\xi,t)\mathcal{A}_2(\xi,t)+u\ (\partial^2u/\partial\xi^2)(\partial\mathcal{A}_2/\partial\xi)\right]}{W(\xi,t)}d\xi$$

$$-\left[\left(\frac{\partial \mathcal{A}_2}{\partial x}\right)_e+\left(\frac{1}{A}\frac{dA}{dx}\right)_e(\mathcal{A}_2)_e\right]$$
$$\times\int_{x_i}^{x_e}\frac{\left[\overline{s}(\xi,t)\mathcal{A}_1(\xi,t)+u\ (\partial^2u/\partial\xi^2)(\partial\mathcal{A}_1/\partial\xi)\right]}{W(\xi,t)}d\xi \tag{B4}$$

The time dependent functions $K_1(t)$ and $K_2(t)$ for case (a) and case (b) boundary conditions in quasi-one-dimensional flows then follow as :

*Case(a): The inlet flow speed and exit pressure are specified.*

In this case, the functions $K_1(t)$ and $K_2(t)$ satisfy the eqs.

$$K_1(t)(\mathcal{A}_1)_i+K_2(t)(\mathcal{A}_2)_i=a_i(t)=\frac{dU_i}{dt} \tag{B5}$$

$$K_1(t)\left[\left(\frac{\partial \mathcal{A}_1}{\partial x}\right)_e+\left(\frac{1}{A}\frac{dA}{dx}\right)_e(\mathcal{A}_1)_e\right]$$
$$+K_2(t)\left[\left(\frac{\partial \mathcal{A}_2}{\partial x}\right)_e+\left(\frac{1}{A}\frac{dA}{dx}\right)_e(\mathcal{A}_2)_e\right]=Q_e(t) \tag{B6}$$

whose solution is given by

$$K_1(t)=\frac{\left[\left(\frac{\partial \mathcal{A}_2}{\partial x}\right)_e+\left(\frac{1}{A}\frac{dA}{dx}\right)_e(\mathcal{A}_2)_e\right]\frac{dU_i}{dt}-(\mathcal{A}_2)_iQ_e}{\Delta_a(t)} \tag{B7}$$

and

$$K_2(t)=-\frac{\left[\left(\frac{\partial \mathcal{A}_1}{\partial x}\right)_e+\left(\frac{1}{A}\frac{dA}{dx}\right)_e(\mathcal{A}_1)_e\right]\frac{dU_i}{dt}-(\mathcal{A}_1)_iQ_e}{\Delta_a(t)} \tag{B8}$$

where $\Delta_a(t)$ is given by

$$\Delta_a(t)=(\mathcal{A}_1)_i\left(\frac{\partial \mathcal{A}_2}{\partial x}\right)_e-(\mathcal{A}_2)_i\left(\frac{\partial \mathcal{A}_1}{\partial x}\right)_e$$
$$+\left(\frac{1}{A}\frac{dA}{dx}\right)_e\left[(\mathcal{A}_1)_i(\mathcal{A}_2)_e-(\mathcal{A}_2)_i(\mathcal{A}_1)_e\right] \tag{B9}$$

*Case(b): The inlet and exit pressures are specified.*

In this case, the functions $K_1(t)$ and $K_2(t)$ satisfy the eqs.

$$K_1(t)\left[\left(\frac{\partial \mathcal{A}_1}{\partial x}\right)_i+\left(\frac{1}{A}\frac{dA}{dx}\right)_i(\mathcal{A}_1)_i\right]$$
$$+K_2(t)\left[\left(\frac{\partial \mathcal{A}_2}{\partial x}\right)_i+\left(\frac{1}{A}\frac{dA}{dx}\right)_i(\mathcal{A}_2)_i\right]=Q_i(t) \tag{B10}$$

and

$$K_1(t)\left[\left(\frac{\partial \mathcal{A}_1}{\partial x}\right)_e+\left(\frac{1}{A}\frac{dA}{dx}\right)_e(\mathcal{A}_1)_e\right]$$
$$+K_2(t)\left[\left(\frac{\partial \mathcal{A}_2}{\partial x}\right)_e+\left(\frac{1}{A}\frac{dA}{dx}\right)_e(\mathcal{A}_2)_e\right]=Q_e(t) \tag{B11}$$

whose solution is given by

$$K_1(t)=\left\{\left[\left(\frac{\partial \mathcal{A}_2}{\partial x}\right)_e+\left(\frac{1}{A}\frac{dA}{dx}\right)_e(\mathcal{A}_2)_e\right]Q_i\right.$$
$$\left.-\left[\left(\frac{\partial \mathcal{A}_2}{\partial x}\right)_i+\left(\frac{1}{A}\frac{dA}{dx}\right)_i(\mathcal{A}_2)_i\right]Q_e\right\}\left[\Delta_b(t)\right]^{-1} \tag{B12}$$

and

$$K_2(t)=-\left\{\left[\left(\frac{\partial \mathcal{A}_1}{\partial x}\right)_e+\left(\frac{1}{A}\frac{dA}{dx}\right)_e(\mathcal{A}_1)_e\right]Q_i\right.$$
$$\left.-\left[\left(\frac{\partial \mathcal{A}_1}{\partial x}\right)_i+\left(\frac{1}{A}\frac{dA}{dx}\right)_i(\mathcal{A}_1)_i\right]Q_e\right\}\left[\Delta_b(t)\right]^{-1} \tag{B13}$$

where $\Delta_b(t)$ is given by

$$\Delta_b(t) = \left[\left(\frac{\partial \mathcal{A}_1}{\partial x}\right)_i + \left(\frac{1}{A}\frac{dA}{dx}\right)_i (\mathcal{A}_1)_i\right]\left[\left(\frac{\partial \mathcal{A}_2}{\partial x}\right)_e + \left(\frac{1}{A}\frac{dA}{dx}\right)_e (\mathcal{A}_2)_e\right]$$

$$- \left[\left(\frac{\partial \mathcal{A}_1}{\partial x}\right)_e + \left(\frac{1}{A}\frac{dA}{dx}\right)_e (\mathcal{A}_1)_e\right]\left[\left(\frac{\partial \mathcal{A}_2}{\partial x}\right)_i + \left(\frac{1}{A}\frac{dA}{dx}\right)_i (\mathcal{A}_2)_i\right] . \tag{B14}$$

## NOMENCLATURE

### Latin

| | | |
|---|---|---|
| $A$ | = | cross-sectional area of the nozzle |
| $C_p$ | = | pressure coefficient |
| $H$ | = | height of nozzle |
| $R$ | = | bubble radius |
| $Re$ | = | flow Reynolds number |
| $S$ | = | surface tension coefficient |
| $U$ | = | flow speed |
| $L$ | = | micro to macro scale |
| $k$ | = | polytropic exponent |
| $p$ | = | mixture pressure |
| $t$ | = | time coordinate |
| $x$ | = | nozzle axial coordinate |
| $y$ | = | nozzle |
| $u$ | = | x-component of velocity field |
| $v$ | = | y-component of velocity field |
| $a$ | = | x-component of unsteady acceleration field |
| $b$ | = | y-component of unsteady acceleration field |
| $f$ | = | shedding frequency |

### Greek

| | | |
|---|---|---|
| $\beta$ | = | void fraction |
| $\mu_{eff}$ | = | effective viscosity of liquid |
| $\eta_0$ | = | number density of nuclei per unit liquid volume |
| $\rho$ | = | mixture density |
| $\psi$ | = | dilation |
| $\omega$ | = | vorticity |
| $\kappa_i$ | = | parameter in terms of inlet void fraction |
| $\Lambda$ | = | bubble-bubble interaction parameter |

### Subscripts

| | | |
|---|---|---|
| $e$ | = | nozzle exit |
| $g$ | = | gas |
| $i$ | = | nozzle inlet |
| $o$ | = | initial |
| $\ell$ | = | liquid phase |
| $sat$ | = | saturated state |
| $v$ | = | vapor phase |

### Superscripts

| | | |
|---|---|---|
| $'$ | = | signifies a dimensional quantity (otherwise dimensionless) |

## REFERENCES


[1] Tangren, R.F., Dodge, C.H. and Seifert, H.S., 1949, "Compressibility effects in two-phase flow," J. Appl. Phys. **20**, 637-645.

[2] Ishii, R., Umeda, Y., Murata, S. and Shishido, N., 1993, "Bubbly flows through a converging-diverging nozzle," Phys. Fluids A 5, 1630-1643.

[3] van Wijngaarden, L., 1968, "On the equations of motion for mixtures of liquid and gas bubbles," J. Fluid Mech. **33**, 465-474.

[4] van Wijngaarden, L., 1972, "One-dimensional flow of liquids containing small gas bubbles," Ann. Rev. Fluid Mech. **4**, 369-396.

[5] Noordzij, L. and van, Wijngaarden, L., 1974, "Relaxation effects, caused by the relative motion, on shock waves in gas-bubble/liquid mixtures," J. Fluid Mech. **66**, 115-143.

[6] Wang, Y. C., and Brennen, C. E., 1998, "One Dimensional Bubbly Cavitating Flows Through a Converging-Diverging Nozzle," ASME J. Fluids Eng., **120**, pp. 166–170.

[7] Delale, C. F., Schnerr, G. H., and Sauer, J., 2001, "Quasi-One-Dimensional Steady-State Cavitating Nozzle Flows," J. Fluid Mech., **427**, pp. 167–204.

[8] Pasinlioğlu,Ş., Delale, C.F. and Schnerr, G.H., 2009, "On the Temporal Stability of Quasi-One-Dimensional Steady-State Bubbly Cavitating Nozzle Flow Solutions, " IMA Journal of Applied Mathematics, **74**, pp. 230-249.

[9] Preston, A. T., Colonius, T., and Brennen, C. E., 2002, "A Numerical Investigation of Unsteady Bubbly Cavitating Nozzle Flows," Phys. Fluids, **14**, pp. 300–311.

[10] Saffman, P.G., 1995, Vortex Dynamics, Cambridge University Press, Cambridge.

[11] Schnerr, G.H., Schmidt, S., Sezal, I and Thalhamer,M., 2006, "Shock and Wave Dynamics of Compressible Liquid Flows Special Emphasis on Unsteady Load on Hydrofoils and on Cavitation in Injection Nozzles," (invited lecture) In: Proceedings of the Sixth International Symposium on Cavitation. Wageningen, The Netherlands, September 11-15, 2006 (CD ROM, ed. G.Kuiper).

[12] Schmidt, S.J., Sezal, I.H., Schnerr, G.H. and Thalhamer, M., 2008, "Riemann Techniques for the Simulation of Compressible Liquid Flows with Phase-Transition at all Mach Numbers - Shock and Wave Dynamics in 3-D Micro and Macro Systems," In: 46th AIAA Aerospace Sciences Meeting and Exhibit, Reno, Nevada, USA, January 7 - 10, AIAA paper 2008-1238, 2008.

[13] Schnerr, G.H., Sezal, I.H., Schmidt, S.J., 2008, "Numerical Investigation of Three-dimensional Cloud Cavitation with Special Emphasis on Collapse Induced Shock Dynamics," Phys. Fluids, Vol. **20**, Issue **4**, 040703, 2008.

[14] Schnerr, G.H., Schmidt, S., Sezal, I and Thalhamer,M., 2009, "Shock and Wave Dynamics in Cavitating Compressible Liquid Flows in Injection Nozzles," Shock Waves, DOI 10.1007/s00193-008-0185-3, 2009.

[15] Brennen, C.E, 1995, Cavitation and Bubble Dynamics, Oxford University Press, Oxford.

[16] Wang, Y.C. and Chen, E., 2002, "Effect of Phase Relative Motion on Critical Bubbly Flows Through a Converging-Diverging Nozzle," Phys. Fluids **14**, 3215-3223.

[17] Mørch, K. A., 2000, "Cavitation Nuclei and Bubble Formation: A Dynamic Liquid-Solid Interface Problem," ASME J. Fluids Eng., **122**, pp. 494–498.
[18] Delale, C. F., Hruby J., and Marsik, F., 2003, "Homogeneous Bubble Nucleation in Liquids: The Classical Theory Revisited," J. Chem. Phys., **118**, pp. 792–906.
[19] Delale, C. F., Okita K., and Matsumoto, Y., 2005, "Steady-State Cavitating Nozzle Flows with Nucleation," ASME J. Fluids Eng., **127**, pp. 770–777.
[20] Brennen, C.E., 2002, "Fission of Collapsing Cavitation Bubbles," J. Fluid Mech., **472**, 153-166.
[21] Delale, C. F., and Tunç, M., 2004, "A Bubble Fission Model for Collapsing Cavitation Bubbles," Phys. Fluids, **16**, pp. 4200–4203.
[22] Blake, J.R. and Gibson, D.C., 1987, "Cavitation Bubbles Near Boundaries," Ann. Rev. Fluid Mech., **19**, 99-123.
[23] Kubota, A., Kato, H. and Yamaguchi, H., 1992, "A numerical study of unsteady cavitation on a hydraulic section," J. Fluid Mech. **240**, 59-96
[24] Nigmatulin, R.I., Khabeev, N.S. and Nagiev, F.B., 1981, "Dynamics, Heat and Mass Transfer of Vapor-Gas Bubbles in a Liquid," Intl. J. Heat Mass Transfer, **24**, 1033-1044-.
[25] Prosperetti, A., Crum, L.A. and Commander, K.W., 1988, "Nonlinear bubble dynamics," J. Acoust. Soc. Am. **83**, 502-514.
[26] Prosperetti, A., 1991, "The Thermal Behavior of Oscillating Gas Bubbles," J. Fluid Mech., **222**, 587-616.
[27] Delale, C. F., 2002, "Thermal Damping in Cavitating Nozzle flows," ASME J. Fluids Eng., **124**, pp. 969–976.
[28] Toro, E.F., 1999, Riemann Solvers and Numerical Methods for Fluid Dynamics: A Practical Introduction, Springer, Heidelberg.
[29] Franc, J.P. and Michel, J.M., 2004, Fundamentals of Cavitation, Kluwer Academic Publishers, Dordrecht, p. 20.